Effective wavelength scaling of rectangular aperture antennas

Yuanyuan Chen, Li Yu, Jiasen Zhang, and Reuven Gordon

April 2015

This article was originally published at:

http://dx.doi.org/10.1364/OE.23.010385

Effective wavelength scaling of rectangular aperture antennas

Yuanyuan Chen,[1,2] Li Yu,[1] Jiasen Zhang,[3] and Reuven Gordon [2,*]

[1]*State Key Lab of Information Photonics and Optical Communications, Department of Science, Beijing University of posts and Telecommunications, Beijing 100876, China*
[2]*Department of Electrical and Computer Engineering, University of Victoria, Victoria, BC, V8W 3V6, Canada*
[3]*State Key Lab for Mesoscopic Physics, Department of Physics, Peking University, Beijing 100871, China*
[*]*rgordon@uvic.ca*

Abstract: We investigate the resonances of aperture antennas from the visible to the terahertz regime, with comparison to comprehensive simulations. Simple piecewise analytic behavior is found for the wavelength scaling over the entire spectrum, with a linear regime through the visible and near-IR. This theory will serve as a useful and simple design tool for applications including biosensors, nonlinear plasmonics and surface enhanced spectroscopies.

OCIS codes: (240.6680) Surface plasmons; (050.1220) Apertures; (140.4780) Optical resonators.

References and links

1. A. Kumar and H. D. Hristov, *Microwave Cavity Antennas* (Academic, 1989).
2. C. Genet and T. W. Ebbesen, "Light in tiny holes," Nature **445**(7123), 39–46 (2007).
3. P. Bharadwaj, B. Deutsch, and L. Novotny, "Optical antennas," Adv. Opt. Photon. **1**(3), 438–483 (2009).
4. J. A. Schuller, E. S. Barnard, W. Cai, Y. C. Jun, J. S. White, and M. L. Brongersma, "Plasmonics for extreme light concentration and manipulation," Nat. Mater. **9**(3), 193–204 (2010).
5. L. Novotny and N. Van Hulst, "Antennas for light," Nat. Photonics **5**(2), 83–90 (2011).
6. P. Mühlschlegel, H.-J. Eisler, O. J. F. Martin, B. Hecht, and D. W. Pohl, "Resonant optical antennas," Science **308**(5728), 1607–1609 (2005).
7. P. Ghenuche, S. Cherukulappurath, T. H. Taminiau, N. F. van Hulst, and R. Quidant, "Spectroscopic mode mapping of resonant plasmon nanoantennas," Phys. Rev. Lett. **101**(11), 116805 (2008).
8. G. W. Bryant, F. J. García de Abajo, and J. Aizpurua, "Mapping the plasmon resonances of metallic nanoantennas," Nano Lett. **8**(2), 631–636 (2008).
9. H. Guo, T. P. Meyrath, T. Zentgraf, N. Liu, L. Fu, H. Schweizer, and H. Giessen, "Optical resonances of bowtie slot antennas and their geometry and material dependence," Opt. Express **16**(11), 7756–7766 (2008).
10. Y. Alaverdyan, B. Sepúlveda, L. Eurenius, E. Olsson, and M. Käll, "Optical antennas based on coupled nanoholes in thin metal films," Nat. Phys. **3**(12), 884–889 (2007).
11. P. Biagioni, J.-S. Huang, and B. Hecht, "Nanoantennas for visible and infrared radiation," Rep. Prog. Phys. **75**(2), 024402 (2012).
12. F. J. García-Vidal, L. Martin-Moreno, T. W. Ebbesen, and L. Kuipers, "Light passing through subwavelength apertures," Rev. Mod. Phys. **82**(1), 729–787 (2010).
13. L. Novotny, "Effective wavelength scaling for optical antennas," Phys. Rev. Lett. **98**(26), 266802 (2007).
14. E.-S. Kwak, T.-D. Onuta, D. Amarie, R. Potyrailo, B. Stein, S. C. Jacobson, W. L. Schaich, and B. Dragnea, "Optical trapping with integrated near-field apertures," J. Phys. Chem. B **108**(36), 13607–13612 (2004).
15. M. L. Juan, R. Gordon, Y. Pang, F. Eftekhari, and R. Quidant, "Self-induced Back-action optical trapping of dielectric nanoparticles," Nat. Phys. **5**(12), 915–919 (2009).
16. M. L. Juan, M. Righini, and R. Quidant, "Plasmon nano-optical tweezers," Nat. Photonics **5**(6), 349–356 (2011).
17. C. Chen, M. L. Juan, Y. Li, G. Maes, G. Borghs, P. Van Dorpe, and R. Quidant, "Enhanced optical trapping and arrangement of nano-objects in a plasmonic nanocavity," Nano Lett. **12**(1), 125–132 (2012).
18. A. Kotnala and R. Gordon, "Quantification of high-efficiency trapping of nanoparticles in a double nanohole optical tweezer," Nano Lett. **14**(2), 853–856 (2014).
19. M. Airola, Y. Liu, and S. Blair, "Second-harmonic generation from an array of sub-wavelength metal Apertures," J. Opt. A, Pure Appl. Opt. **7**(2), S118–S123 (2005).
20. A. Lesuffleur, L. K. S. Kumar, and R. Gordon, "Enhanced second harmonic generation from nanoscale double-hole arrays in a gold film," Appl. Phys. Lett. **88**(26), 261104 (2006).
21. T. Xu, X. Jiao, G. P. Zhang, and S. Blair, "Second-harmonic emission from sub-wavelength apertures: Effects of aperture symmetry and lattice arrangement," Opt. Express **15**(21), 13894–13906 (2007).
22. T. Xu, X. Jiao, and S. Blair, "Third-harmonic generation from arrays of sub-wavelength metal apertures," Opt. Express **17**(26), 23582–23588 (2009).

#232897 - $15.00 USD Received 20 Jan 2015; revised 3 Apr 2015; accepted 7 Apr 2015; published 14 Apr 2015

23. B. L. Wang, R. Wang, R. J. Liu, X. H. Lu, J. Zhao, and Z. Y. Li, "Origin of shape resonance in second-harmonic generation from metallic nanohole arrays," Sci. Rep. **3**, 2358 (2013).
24. A. Salomon, M. Zielinski, R. Kolkowski, J. Zyss, and Y. Prior, "Size and shape resonances in second harmonic generation from silver nanocavities," J. Phys. Chem. C **117**(43), 22377–22382 (2013).
25. T. Rindzevicius, Y. Alaverdyan, A. Dahlin, F. Höök, D. S. Sutherland, and M. Käll, "Plasmonic sensing characteristics of single nanometric holes," Nano Lett. **5**(11), 2335–2339 (2005).
26. A. Dahlin, M. Zäch, T. Rindzevicius, M. Käll, D. S. Sutherland, and F. Höök, "Localized surface plasmon resonance sensing of lipid-membrane-mediated biorecognition events," J. Am. Chem. Soc. **127**(14), 5043–5048 (2005).
27. K. A. Tetz, L. Pang, and Y. Fainman, "High-resolution surface plasmon resonance sensor based on linewidth-optimized nanohole array transmittance," Opt. Lett. **31**(10), 1528–1530 (2006).
28. M. E. Stewart, C. R. Anderton, L. B. Thompson, J. Maria, S. K. Gray, J. A. Rogers, and R. G. Nuzzo, "Nanostructured plasmonic sensors," Chem. Rev. **108**(2), 494–521 (2008).
29. K. M. Mayer and J. H. Hafner, "Localized surface plasmon resonance sensors," Chem. Rev. **111**(6), 3828–3857 (2011).
30. A. G. Brolo, E. Arctander, R. Gordon, B. Leathem, and K. L. Kavanagh, "Nanohole-enhanced raman scattering," Nano Lett. **4**(10), 2015–2018 (2004).
31. Q. Yu, P. Guan, D. Qin, G. Golden, and P. M. Wallace, "Inverted size-dependence of surface-enhanced Raman scattering on gold nanohole and nanodisk arrays," Nano Lett. **8**(7), 1923–1928 (2008).
32. D. Gérard, J. Wenger, N. Bonod, E. Popov, H. Rigneault, F. Mahdavi, S. Blair, J. Dintinger, and T. W. Ebbesen, "Nanoaperture-enhanced fluorescence: Towards higher detection rates with plasmonic metals," Phys. Rev. B **77**(4), 045413 (2008).
33. F. J. García-Vidal, E. Moreno, J. A. Porto, and L. Martín-Moreno, "Transmission of light through a single rectangular hole," Phys. Rev. Lett. **95**(10), 103901 (2005).
34. J. R. Suckling, A. P. Hibbins, M. J. Lockyear, T. W. Preist, J. R. Sambles, and C. R. Lawrence, "Finite conductance governs the resonance transmission of thin metal slits at microwave frequencies," Phys. Rev. Lett. **92**(14), 147401 (2004).
35. F. J. García-Vidal, L. Martín-Moreno, E. Moreno, L. K. S. Kumar, and R. Gordon, "Transmission of light through a single rectangular hole in a real metal," Phys. Rev. B **74**(15), 153411 (2006).
36. A. Degiron, H. J. Lezec, N. Yamamoto, and T. W. Ebbesen, "Optical transmission properties of a single subwavelength aperture in a real metal," Opt. Commun. **239**(1-3), 61–66 (2004).
37. J.-H. Choe, J. H. Kang, D. S. Kim, and Q. H. Park, "Slot antenna as a bound charge oscillator," Opt. Express **20**(6), 6521–6526 (2012).
38. R. Gordon and A. Brolo, "Increased cut-off wavelength for a subwavelength hole in a real metal," Opt. Express **13**(6), 1933–1938 (2005).
39. R. Gordon, "Light in a subwavelength slit in a metal: propagation and reflection," Phys. Rev. B **73**(15), 153405 (2006).
40. M. S. Tame, K. R. McEnery, S. K. Ozdemir, J. Lee, S. A. Maier, and M. S. Kim, "Quantum plasmonics," Nat. Phys. **9**(6), 329–340 (2013).
41. G. Hajisalem, M. S. Nezami, and R. Gordon, "Probing the quantum tunneling limit of plasmonic enhancement by third harmonic generation," Nano Lett. **14**(11), 6651–6654 (2014).
42. D. C. Marinica, A. K. Kazansky, P. Nordlander, J. Aizpurua, and A. G. Borisov, "Quantum plasmonics: Nonlinear effects in the field enhancement of a plasmonic nanoparticle dimer," Nano Lett. **12**(3), 1333–1339 (2012).
43. J. Braun, B. Gompf, G. Kobiela, and M. Dressel, "How holes can obscure the view: suppressed transmission through an ultrathin metal film by a subwavelength hole array," Phys. Rev. Lett. **103**(20), 203901 (2009).
44. N. Bonod, S. Enoch, L. Li, P. Evgeny, and M. Nevière, "Resonant optical transmission through thin metallic films with and without holes," Opt. Express **11**(5), 482–490 (2003).
45. P. B. Johnson and R. W. Christy, "Optical constants of the noble metals," Phys. Rev. B **6**(12), 4370–4379 (1972).
46. R. Gordon, L. K. S. Kumar, and A. G. Brolo, "Resonant light transmission through a nanohole in a metal film," IEEE Trans. NanoTechnol. **5**(3), 291–294 (2006).

1. Introduction

An antenna is a structure that efficiently couples electromagnetic energy between the near-field and the radiation zone. For example, a microwave rectangular aperture antenna is designed to have the long edge equal to half the free-space wavelength of operation [1]. A nanoantenna, or optical antenna [2–5], performs this task using nanostructured metals and down to visible and shorter wavelengths. Due to the small size of nanoantennas, the dispersion properties of modes acting in the antenna are strongly influenced by proximity effects [6–8]. Hence, a nanoantenna no longer works at wavelengths comparable to the size of the antenna so it is necessary to introduce an effective wavelength to aid in antenna design, which depends on the material and structural properties [9–12]. In one of the most influential plasmonics papers, it was shown that the wavelength, λ, is scaled down due to the plasmonic

#232897 - $15.00 USD Received 20 Jan 2015; revised 3 Apr 2015; accepted 7 Apr 2015; published 14 Apr 2015

dispersion of a single antenna segment (cylindrical rod) [13]. Similar effects are expected to arise for aperture antennas that have particularly important applications, such as optical tweezers [14–18], nonlinear optics [19–24], sensing [25–29] and SERS [30–32].

While several works have considered the optical properties of nanoholes [33–37], those works have not provided straightforward design rules as was found for nanorods [13]. Here, we derive the simple scaling law for the aperture antenna in the wide wavelength range from the visible to THz. Similar to the works that have focused on waveguide dispersion on nanorods, the scaling in this paper is based on a theory that incorporates the dispersion of the mode inside the aperture where the permittivity of the metal is taken into account. The theory gives a simple result that shows how, for the single aperture perforated on a real metal film, the width of rectangular nanohole and the wavelength of operation affects the resonant response over a broad spectral range.

2. Theoretical approach

Figure 1 shows schematically the system under consideration. A rectangular aperture of short edge W and long edge L perforated on a gold film of thickness T is analyzed. The center of the hole is assumed to be air. The metal has relative permittivity $\varepsilon_m(\lambda)$ that can be modeled according to the Drude theory. The system is illuminated by a normally incident plane wave with the free-space wavelength λ, and the in-plane component of the electric field pointing along the x direction.

As has been considered in previous works [36–39], the waveguide mode of a subwavelength rectangular hole in a real metal is analyzed by using the surface plasmon waveguide dispersion theory. For a single rectangular aperture, the resonance is influenced by both coupling between SP modes along the x-direction and penetration of the field into the metal along the y-direction. We seek the waveguide cut-off to identify the antenna resonance, as is described in more detail in the Appendix. To identify the two separate contributions to the resonant wavelength, we break the 2D problem down into two 1D effective-index problems as shown in Fig. 1. Along the x-direction, the lowest-order mode is analyzed by considering the TM mode of a slab of width W, to derive an effective dielectric constant. Along the y-direction, the TE mode component in a slab of separation L filled with the effective dielectric (ε_d) is analyzed. The propagation constant, β_{TE}, of the TE mode between two parallel plates of a real metal can be found from the characteristic equation:

$$\tan\left(\sqrt{k_0^2\varepsilon_d-\beta_{TE}^2}\,\frac{L}{2}\right)=\frac{\sqrt{\beta_{TE}^2-k_0^2\varepsilon_m}}{\sqrt{k_0^2\varepsilon_d-\beta_{TE}^2}} \tag{1}$$

Where L is the length of the aperture, k_0 is the free-space wave-vector, ε_m is the relative permittivity of the metal, ε_d is the relative permittivity of the dielectric between the metal sides. Here we use the effective permittivity $\varepsilon_d=\left(\frac{\beta_{TM}}{k_0}\right)^2$ to capture the influence of the SP gap mode (where β_{TM} is the propagation constant of the TM gap mode). By setting the overall propagation constant, β_{TE}, to zero, we can find the length of the aperture at resonance:

$$L=\frac{2}{k_0\sqrt{\varepsilon_{\mathrm{d}}}}\arctan\left(\sqrt{-\frac{\varepsilon_m}{\varepsilon_d}}\right) \tag{2}$$

The effective wavelength is now calculated as:

#232897 - $15.00 USD Received 20 Jan 2015; revised 3 Apr 2015; accepted 7 Apr 2015; published 14 Apr 2015

$$\lambda_{eff} = 2L = \frac{4}{\beta_{TM}} \arctan\left(\frac{k_0}{\beta_{TM}}\sqrt{-\varepsilon_m}\right) \tag{3}$$

It should be noted that the effective wavelength is twice the length of the aperture that gives the resonance. The reason for this convention is to show the wavelength scaling with respect to the perfect electric conductor case. For TM modes, the characteristic equation for this configuration is modified from the dielectric case to be:

$$\tanh\left(\sqrt{\beta_{TM}{}^2 - k_0{}^2\varepsilon_{air}}\,\frac{W}{2}\right) = -\frac{\varepsilon_{air}}{\varepsilon_m}\frac{\sqrt{\beta_{TM}{}^2 - k_0{}^2\varepsilon_m}}{\sqrt{\beta_{TM}{}^2 - k_0{}^2\varepsilon_{air}}} \tag{4}$$

Where ε_{air} is the permittivity of air and W is the width of aperture. Here, we consider an aperture perforated on a gold film characterized by a free electron gas according to the Drude formula:

$$\varepsilon_m = \varepsilon_\infty - \frac{\omega_p{}^2}{\omega^2 + i\gamma\omega} \tag{5}$$

Where ε_∞ is the infinite frequency limit of the dielectric function, ω_p is the plasma frequency and $\gamma = \frac{1}{\tau}$ is characteristic collision frequency. τ is the relaxation time of the free electrons. For gold, $\varepsilon_\infty \approx 11$, $\omega_p = 1.37\text{e}16$ Hz and $\gamma = 1.05\text{e}14$ Hz.

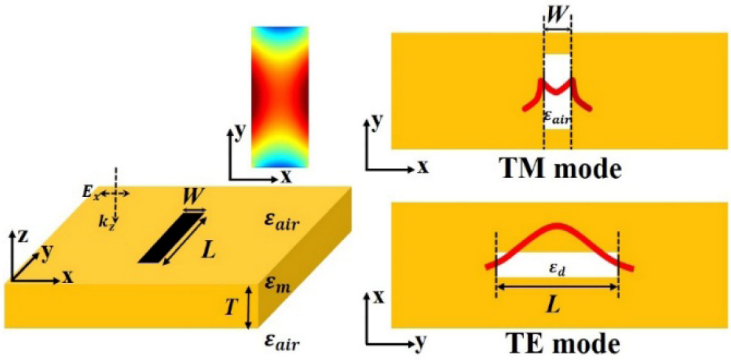

Fig. 1. Diagram of a single rectangular aperture of sides W and L in a metal of thickness T, with co-ordinates shown. The structure is illuminated by a normally incident plane wave with its E-field vector pointing along the x axis. The inset is E-field amplitude evaluated at the resonant wavelength. The lowest-order mode is analyzed for TM mode along the x axis. The TE mode component along the y axis with the effective dielectric is then calculated.

Figure 2(a) shows the λ_{eff} versus λ for rectangular aperture with four different values of W = 30, 50, 300 and 500 nm (as calculated from Eqs. (1)-(5)). Here we use the log-log scale. In these four cases, λ_{eff} are all relatively shorter than λ due to the finite permittivity of the metal. For example, for the aperture antenna (L = 143 nm, W = 30 nm) one calculates $\lambda_{eff} = \lambda / 2.45$. For the aperture antenna (L = 253 nm, W = 500 nm) one calculates $\lambda_{eff} = \lambda / 1.32$. In addition, it is clear that there is a close correlation between the λ_{eff} and the value of W. For the case of a rectangular hole with relatively wide width (e.g. W = 500 nm), the effective wavelength almost follows from a simple linear scaling of the free-space wavelength in a wide wavelength regime. However, when the width scales down to the

#232897 - $15.00 USD Received 20 Jan 2015; revised 3 Apr 2015; accepted 7 Apr 2015; published 14 Apr 2015

order of tens of nanometers (e.g. W = 30 nm), the linear relation between the λ and λ_{eff} breaks down at longer wavelengths. This deviation at longer wavelengths occurs when the dimensions of the structure are of the order of (or smaller than) the skin depth or penetration into the metal. We calculate when the skin depth is equal to the width of aperture antenna. As shown in Fig. 2(a) with a vertical line, it is almost the same regime where the deviation occurs for longer wavelengths. In addition, the nonlinear part in the short wavelength is caused by the surface plasmon resonance of the metal film leading to a divergent β_{TM} , which occurs when approaching the angular frequency $\omega_{sp}/\sqrt{2}$.

To validate the analytical approach, we use finite-difference time-domain (FDTD) numerical calculations on this structure. In the simulation, the source used is a plane wave. The thickness of the gold film is 100 nm. The width of rectangular aperture is W = 30 nm, 50 nm and 500 nm. Convergence was ensured by reducing the grid-size and extending the artificial PEC boundaries. The smallest grid-size attempted was 1 nm. As shown in Fig. 2(b), the theoretical derivation for the effective wavelength gives very accurate results when compared with the FDTD calculations. The smallest size for the width of antenna we used is 30 nm and good agreement is found between the theoretical derivation and the FDTD calculations. This value was used based on what is practical to fabricate in optically thick metal films. We expect that theory will hold down to sub-nanometer sizes where the dispersion relation is valid; however, for sub-nanometer gaps tunneling will start to play a role and modify the dispersion [40–42].

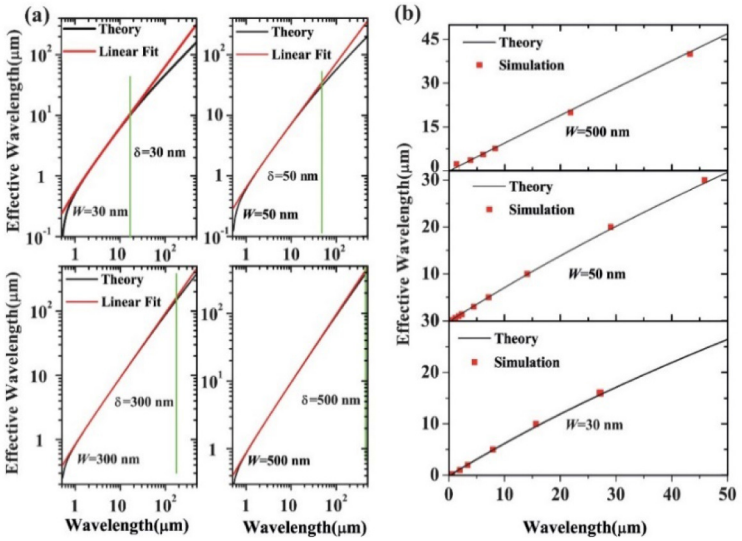

Fig. 2. (a) The effective wavelength versus free-space wavelength for rectangular aperture with four different values of W = 30, 50, 300 and 500 nm in gold. The black lines are theory results calculated from Eqs. (1)-(5). The red lines are the linear approximation to the theory results. The vertical green lines represent the positon where the skin depth is equal to the width of aperture. (b) The effective wavelength for rectangular holes as calculated using the effective index method. The ■ points give the result from numerical simulations.

3. Scaling from visible to near-IR regimes

In the next two sections, we derive a simple scaling law of λ_{eff} for the aperture antenna in the wide wavelength range (from the visible to the THz). For the rectangular aperture, the propagation constant β_{TM} of TM_0 modes are solutions of Eq. (4), which can also be expressed as:

#232897 - $15.00 USD Received 20 Jan 2015; revised 3 Apr 2015; accepted 7 Apr 2015; published 14 Apr 2015

$$1-\frac{2}{1+e^{-W\sqrt{\beta_{TM}{}^2-k_0{}^2}}}=\frac{\varepsilon_{air}}{\varepsilon_m}\frac{\sqrt{\beta_{TM}{}^2-k_0{}^2\varepsilon_m}}{\sqrt{\beta_{TM}{}^2-k_0{}^2\varepsilon_{air}}} \tag{6}$$

Due to the $W \ll \lambda$, we use the approximation for $\frac{1}{1+e^{-W\sqrt{\beta_{TM}{}^2-k_0{}^2}}}$ here and obtain to lowest order on $\frac{W}{\lambda}$. Thus, β_{TM} is calculated as:

$$\beta_{TM}{}^2=k_0{}^2+\frac{2}{W^2\varepsilon_m{}^2}-\frac{2}{W\varepsilon_m}\sqrt{\frac{1}{W^2\varepsilon_m{}^2}+(1-\varepsilon_m)k_0{}^2} \tag{7}$$

For the short wavelength range, we consider the real metals characterized by a free electron gas according to the Drude formula (ignoring losses in Eq. (5)):

$$\varepsilon_m=\varepsilon_\infty-\frac{\lambda^2}{\lambda_P{}^2} \tag{8}$$

After inserting the Eq. (8) into Eq. (7), we expand the latter of Eq. (7) in powers of $(\frac{\lambda_P{}^2}{\lambda^2})$ and obtain to lowest order. Equation (7) can now reduce to:

$$\beta_{TM}{}^2=k_0{}^2+\frac{2}{W^2\varepsilon_m{}^2}-\frac{4\pi}{W\varepsilon_m\lambda_p}-\frac{2(1-\varepsilon_\infty)\pi\lambda_p}{W\varepsilon_m\lambda^2} \tag{9}$$

For $\frac{k_0}{\beta_{TM}}\sqrt{-\varepsilon_m} \gg 1$, Eq. (3) can be simplified to:

$$\lambda_{eff}=\frac{4}{\beta_{TM}}\left(\frac{\pi}{2}-\arctan\left(\frac{\beta_{TM}}{k_0\sqrt{-\varepsilon_m}}\right)\right)\approx\frac{2\pi}{\beta_{TM}}-\frac{(\pi+0.75)}{k_0\sqrt{-\varepsilon_m}} \tag{10}$$

Inserting the Eq. (9) into Eq. (10) and after a few arrangements we find the simple scaling law of λ_{eff}:

$$\lambda_{eff}=\sqrt{\frac{\lambda'}{a_1+a_2\frac{1}{\lambda'-\varepsilon_\infty}}}-a_3\sqrt{\frac{\lambda'}{\lambda'-\varepsilon_\infty}} \tag{11}$$

Here, $\lambda'=\frac{\lambda^2}{\lambda_P{}^2}$, a_1, a_2 and a_3 are constant which are related to the width of slit.

$$a_1=\frac{1}{\lambda_P{}^2}+\frac{1}{\pi\lambda_P W}$$

$$a_2=\frac{(\varepsilon_\infty+1)}{2W\pi\lambda_P}$$

$$a_3=\frac{(\pi+0.75)\lambda_P}{2\pi}$$

#232897 - $15.00 USD Received 20 Jan 2015; revised 3 Apr 2015; accepted 7 Apr 2015; published 14 Apr 2015

Using Taylor expansion, we get the simple linear scaling of the free-space wavelength:

$$\lambda_{eff} = \frac{1}{\lambda_P \sqrt{a_1}} \lambda - a_3 \tag{12}$$

Figure 3 shows the comparison based on Eqs. (11) and (12) to the theory data obtained for the aperture with two different values of W = 50 nm and 500 nm. Here we use the log-log scale. Note that the comparison based on Eq. (11) is perfect for the aperture with W = 500 nm, and it is still good even the width of the aperture scaled down to 50 nm. In the case of aperture with W = 50 nm, the comparison breaks down with the theory data when the wavelength is longer than about 25 μm (as shown in the circle). This is because the Drude formula (Eq. (8)) only has the real part of permittivity. However, the imaginary part of the permittivity typically dominates the resonance when the dimensions of the structure are small enough, the order of (or smaller than) the skin depth. Hence the imaginary part of the permittivity needs to be considered, which will be discussed in the next section. In addition, the simple linear scaling based on Eq. (12) also has good agreement with the full theoretical result and is valid over a broad range. As discussed above, the linear relationship between the λ and λ_{eff} breaks down in both the short and long wavelength regimes, thus the linear scaling law only works in limited range.

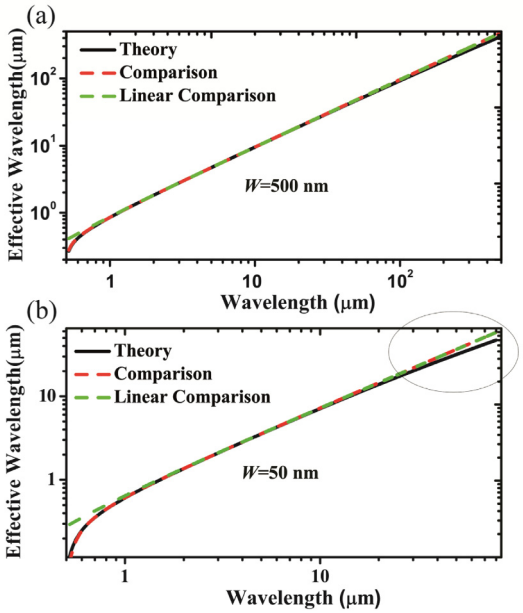

Fig. 3. Effective wavelength for rectangular aperture with two different width W = 50 nm and 500 nm in gold. The log-log scale plot is used. The black curve is calculated according to Eqs. (1)-(5). The red curve is simple scaling law according to Eq. (11). The green curve is the simple linear scaling according to Eq. (12). (a) The comparison regime is from 500 nm-500 μm. (b) The comparison regime is from 500 nm-50 μm.

4. Scaling from infra-red to THz regime

For the aperture antenna with very small width, the use of real part of permittivity is not valid when λ extends to the long wavelength. In this part we take the imaginary part of permittivity into account and derive the scaling law of λ_{eff} for the infra-red to THz regime. When the wavelength is long enough, the real metal can be characterized by the imaginary part of permittivity according to the Drude formula (Eq. (5)):

#232897 - $15.00 USD Received 20 Jan 2015; revised 3 Apr 2015; accepted 7 Apr 2015; published 14 Apr 2015

$$\varepsilon_m = i\frac{{\omega_p}^2\tau}{\omega} \tag{13}$$

Inserting ε_m defined in Eq. (13) into Eq. (7) and after a few arrangements we get the scaling law of λ_{eff} :

$$\lambda_{eff} = \frac{\lambda}{\sqrt{2+2a_1\sqrt{\lambda}}}\sqrt{\frac{1}{1+\frac{1}{(\frac{1}{a_1\sqrt{\lambda}}+1)^2}}+\frac{1}{\sqrt{1+\frac{1}{(\frac{1}{a_1\sqrt{\lambda}}+1)^2}}}-a_2\sqrt{\lambda}} \tag{14}$$

Here, a_1 and a_2 are constants which are related to the width of the slit.

$$a_1 = \frac{\sqrt{c}}{W\omega_p\sqrt{\pi\tau}}$$

$$a_2 = \frac{(\pi+0.75)}{2\omega_p}\sqrt{\frac{c}{\pi\tau}}$$

Figure 4 shows the comparison based on Eq. (14) for the aperture with two different values of W = 50 nm and 500 nm in the THZ wavelength range (100 μm-1000 μm). Here we also use the log-log scale plot. Excellent agreement is found for both the two aperture antennas. Note that for the long wavelength limit, where $\lambda \to \infty$, the effective wavelength goes to $\lambda^{3/4}/\sqrt{2a_1}$, which is different form the perfect electric conductor (PEC) case. This is because for the real metal, the skin depth increases as the wavelength increases, so that the penetration into the metal is greater and the role of the imperfect conductor never goes away. This result shows the value of our theoretical approach in correctly predicting the scaling. Actually, the PEC result can be recovered by setting the scattering time to a large value in Eq. (14); in this limit, $a_1 \to 0, a_2 \to 0$, so that $\lambda_{eff} \to \lambda$.

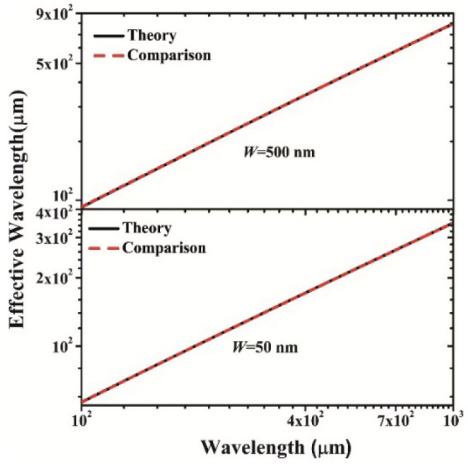

Fig. 4. Effective wavelength for rectangular aperture with two different width W = 50 nm and 500 nm in gold for THZ wavelength (100 μm-1000 μm). The log-log scale plot is used. The black curve is calculated according to Eqs. (1)-(5). The red curve is simple scaling law according to Eq. (14).

#232897 - $15.00 USD Received 20 Jan 2015; revised 3 Apr 2015; accepted 7 Apr 2015; published 14 Apr 2015

Figure 5 renders the fitting Eqs. (11) and (14) in the wide wavelength range (from the optical to THz). Comparing the two figures, we can conclude that the resonant mode in the slit is a coupled surface mode. For the aperture antenna with ultra-narrow width (comparable with the dimensions of the skin depth or penetration into the metal), the influence of the imaginary part of permittivity is dominant.

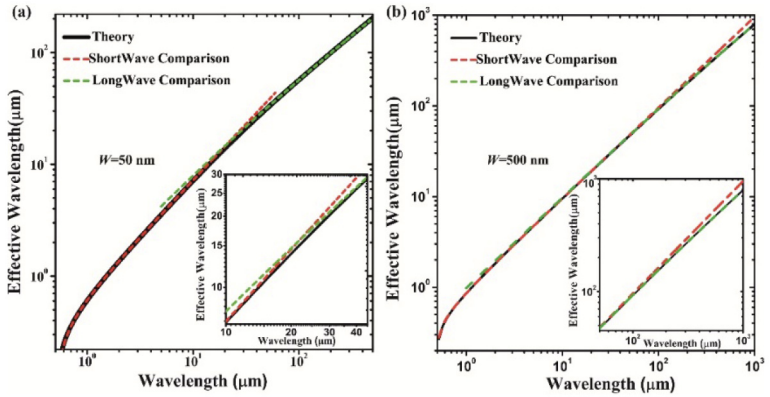

Fig. 5. Effective wavelength for rectangular aperture with two different width W = 50 nm and 500 nm in gold for wide wavelength ranging from the visible to the THz. The log-log scale plot is used. The black curve is calculated according to Eqs. (1)-(5). The red curve is calculated according to Eq. (10). The green curve is calculated according to Eq. (13).

5. Discussion

As shown in Fig. 3, the comparison based on the linear Eq. (11) is good for a wide range of operation. Therefore, the aperture can have an effective wavelength scaling analogous to past works on nanorods [13]. Note that the mismatched part in the short wavelength for the linear comparison and theory is caused by the neglecting higher-order terms in the Eq. (11). The expansion of Eq. (11) is calculated as:

$$\lambda_{eff} = \frac{1}{\lambda_p \sqrt{a_1}} \lambda - a_3 - \frac{\varepsilon_\infty \lambda_p^{\,2}}{4W\pi\sqrt{a_1}} \frac{1}{\lambda} - \frac{\varepsilon_\infty \lambda_p^{\,2} a_3}{2} \frac{1}{\lambda^2} \tag{15}$$

By neglecting the higher-order terms about $\frac{1}{\lambda}$, the comparison for the linear part can be obtained (Eq. (12)), which leads to the mismatch.

The theory presented here is based on surface plasmon waveguide dispersion theory taking into account the finite conductivity. As the slit becomes narrower, the effective index of the mode in the slit increases and the amplitude and phase of the reflection of the mode at the free-space boundary are modified [39]. The theory in this paper asserts that β_{TE}=0, which is the propagation constant in the z direction. This means that there is no dependence on thickness. In practice, however, there is a finite phase of reflection, which will introduce a length dependence using the usual Fabry-Perot (FP) condition, as discussed in the Appendix. Thicker films are actually less sensitive to the end-face reflection. For thin films that allow significant transmission even without apertures, the value of the theory is debatable and indeed apertures can even lead to enhanced absorption [43, 44]. In a past work [13], there was an offset to the wavelength rescaling of the nanorod antenna resonance for the real metal case. This offset arises from two contributions: one is in the dispersion of the metal and the second comes from assuming zero phase reflection at the transition to the semi-spherical end-caps of the nanorod (essentially cutting off the ends and setting the phase to zero).Similarly, here we consider the offset from the dispersion, and we set the phase from the end-terminations to

#232897 - $15.00 USD Received 20 Jan 2015; revised 3 Apr 2015; accepted 7 Apr 2015; published 14 Apr 2015

zero (see Appendix for further discussion). In addition, the metal here is characterized by a free electron gas according to the Drude formula Eq. (5) which is an approximation that is limited by the appearance of interband transitions in real metal systems. This will limit the applicability of our model; however, the analytic simplicity of the results motivate considering the regimes where the Drude model applies. Also, for several metals, there are large wavelength ranges where the Drude model can accurately represent the real metal's dispersion; for example, gold can be accurately represented by the Drude model for wavelengths longer than 600 nm and silver can be accurately represented by the Drude model for wavelengths longer than 350 nm [45].

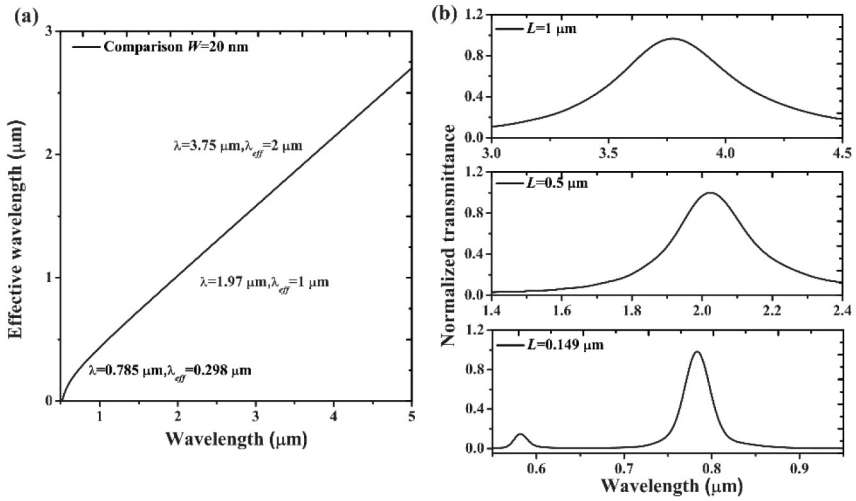

Fig. 6. (a) The effective wavelength versus free-space wavelength for rectangular aperture with W = 20 nm (as calculated from Eq. (11)). (b) Normalized resonant transmission (T) versus wavelength for rectangular apertures with W = 20 nm, L = 149 nm, 500 nm, 1000 nm and T = 100 nm in the simulation.

To demonstrate the developed theory in a design application, we first calculate for the effective wavelength using the operating wavelength (in this case 785 nm) given a desired width of aperture, using Eq. (11). Then we use the half of the effective wavelength to set the length of the aperture in the simulation. Finally, we provide a full simulation to verify that the resonance wavelength is at the desired design wavelength. Figure 6(a) shows the developed scaling theory result based on the comparison with Eq. (11) for the aperture with W = 20 nm. It shows that the effective wavelength of $\lambda_{eff}=2L=0.298\mu m, 1\mu m$ and $2\mu m$ correspond to the incident wavelength of λ=0.785μm, $1.97\mu m$ and $3.75\mu m$ respectively. The latter two values were added to show that the agreement with simulation is good over the entire range of simulation. Here, the width of the apertures are all 20 nm and the aperture antenna is perforated on a gold film of thickness 100 nm. As shown in Fig. 6(b), the spectrum have peaks at $\lambda=0.786\mu m, 2.01\mu m$ $3.77\mu m$, which agree well with the theory results based on the wavelength scaling rule of Eq. (11). (The additional short-wavelength peak in Fig. 6(c), bottom, comes from a higher-order z-direction resonance that we do not discuss in this work.)

6. Conclusions

In summary, we presented an analytic theory for the resonances of a rectangular metallic aperture antenna from the visible to the terahertz regimes. The theory gave a simple result that shows how the width of rectangular nanohole and the wavelength of operation affect the resonant response. The piecewise analytic behavior was found for the wavelength scaling over the entire spectrum. Based on the theoretical analysis, we derived the simple scaling law for the aperture antenna in the wide wavelength range, linear scaling from visible to near-IR

#232897 - $15.00 USD Received 20 Jan 2015; revised 3 Apr 2015; accepted 7 Apr 2015; published 14 Apr 2015

regimes and a simple analytic expression for the THz regimes, as well as short wavelengths. According to the scaling law, we designed a Raman substrate for operation at 785 nm with a 20 nm gap. The scaling results agreed well with finite-difference time-domain numerical calculations. This theory can serve as a simple design tool for nanoapertures with applications including biosensors, nonlinear optics, SERS and photovoltaics.

APPENDIX:

Peak transmission and resonance condition

There are two effects that determine the peak transmission for an aperture. The one is the Fabry-Perot (FP) resonance condition, and the other is the cut-off condition. A FP peak can occur when the phase condition is upheld:

$$\beta_{TE} T + \Phi = m\pi \tag{16}$$

Where T is the film thickness, Φ is the phase of reflection and m is the whole-number resonance order. In this paper, we assume $\Phi = 0$ and $m = 0$. In practice, however, there is a finite phase of reflection, and so $\Phi \neq 0$ gives the resonance condition. For this case:

$$\Delta\beta_{TE} = -\frac{\Phi}{T} \tag{17}$$

We see that the FP resonance is less sensitive to phase-of-reflection for thicker films and will occur closer to the condition used in the main text $\beta_{TE} = 0$.

The cut-off can lead to a transmission peak due to the exponential decay of the field in the aperture above cut-off. For wavelengths longer than cut-off, the light will decay exponentially in the aperture and lead to reduced transmission. This effect is also more pronounced for thicker films since there is more exponential decay. Therefore, the transmission will be larger at β_{TE}=0 than for longer wavelengths and so a peak can appear.

Of course, in the case where the phase of reflection is negative, the FP peak can occur for finite β_{TE} away from cut-off, and we have considered this case with simulations previously [46]; however, this is not captured by the present theory.

Acknowledgments

This work was supported by the National Natural Science Foundation of China under Grant 11374041, the National Basic Research Program of China under Grant 2010CB923202, and the Fund of State Key Laboratory of Information Photonics and Optical Communications of Beijing University of Posts and Telecommunications.

#232897 - $15.00 USD Received 20 Jan 2015; revised 3 Apr 2015; accepted 7 Apr 2015; published 14 Apr 2015